Review of 'Observational evidence of moistening the lowermost stratosphere via isentropic mixing across the subtropical jet' by Langille et al. submitted to Atm. Chem. Phys. (acp-2019-220)

The authors have submitted a reviewed version of their manuscript, much improved and better focused. I think that it can be published after a few minor revisions.

Author response: Thank you for your suggestions and comments. Please find responses to each minor correction in blue below. The marked up manuscript can be found attached as well.

Minor corrections:

L35: Please, include a reference to the description of the SHOW instrument

A reference to Langille et al., 2018 has been included.

L37-41: It is correct to mention here that the goal is to study the event; however, most of this text is a statement on the results that should be moved to the 'Discussions and Conclusions'

We do not believe that the text should be moved to the Discussion and Conclusion section. The statement that we have included clarifies the point of the paper and the importance of the results to the reader. We feel that this is important to include in the introduction.

L43-38: Respectfully, the text in these lines shows careless exposition and writing. No doubt, with 'drop' you want to say that the extratropical tropopause is at an altitude lower than the tropical one. However, saying that it 'drops' is not of a proper explanation about climatological characteristics and the physical mechanisms that drive to such behaviour (that have nothing to do with a 'drop')

The word “drop” may be a bit too colloquial. Therefore, we replace the word “drop” and edit the line to say: “A ubiquitous feature here is a sudden decrease in the altitude of the thermal tropopause”.

L51-52: As it is written right now, it could be understood that wave breaking is the only mechanism associated with it. Please, modify the text to make clear that it is part of the existing possibilities "...is associated (among others) with Rossby-wave breaking and large-scale poleward transport." For example, a nice addition to frame the topic here could be to mention that the increase of vertical baroclinicity is also associated with double-tropopauses. This phenomenon was observed by Castanheira et al. (https://doi.org/10.5194/acp-9-9143-2009) using normal modes (therefore filtering Rossby waves), and it is a well-known impact of global climate change.

The text is meant to focus the reader on the fact that the lowermost atmosphere is strongly influenced by isentropic mixing associated with Rossby wave breaking and that the double tropopause “can” be associated with it. The current wording does not suggest that wave breaking is the only mechanism associated with it. In any case, in order to ensure the text is clear, the line in question has been edited to read: “A number of more recent studies have shown that the occurrence of a double tropopause **can be** associated with Rossby- wave breaking and large-scale poleward transport.” The inclusion of “**can be**” here ensures it is clear that we are not suggesting it is the only mechanism associated with it. Including a broader discussion of other mechanisms responsible for the generation of multiple tropopauses would distract the reader from the point of the paper.

L52: signature?

"Signatures" is used here instead of "signature" since there is indeed more than one type of variability or "signature" imprinted on the spatial distribution of the trace species that can be associated to wave breaking.

L56-65: most of this information is repeated later in Section 2. I suggest to include here only a simple comment on the use of SHOW and refer the reader to such section.

We have removed the quoted lines below since it is repeated in Section 2 and referred the reader to Section 2 for more details on the instrument specifications:

"The instrument implements a limb imaging spatial heterodyne spectrometer (SHS) to obtain vertically resolved images of the water vapour spectrum using limb-scattered sunlight in a 2 nm spectral window centered on 1364.5 nm (Langille et al., 2017). Each SHOW measurement is inverted using the optimal estimation approach to obtain the vertical water vapour profile for each along-track sample (Langille et al., 2018)."

L72: Absolute values are not too informative. I understand that this refers to previous work, but if possible, I would suggest adding relative errors or percentages of bias compared to the values measured by the radiosondes.

A slight positive bias of 3.3% was recorded between the sonde measurements and SHOW presented in early paper. Remaining percent differences are found to be from +/- 10%. Differences between them are expected due to difference in the observed column of air, viewing geometry from SHOW, measurement uncertainty and known issues with the accuracy of the radiosonde at these altitudes. However, as discussed in Langille et al.(2019) differences between the radiosonde and SHOW can be (and were) used to check consistency and general shape (and magnitude) of the profile between the two measurements. The text has been edited to report the %bias and %difference between the measurements as shown below:

"….with the radiosonde recording a positive bias of ~ 3.3% relative to SHOW and percent differences of < ±10 % , due to both natural variability between the observations and measurement precision."

L85-90: I support the view of the authors of avoiding the inclusion of unnecessary discussions in the Introduction. I prefer it too. However, this paper is not so long to consider it unreadable. It is seventeen pages long in its current form, including abstract, twenty-nine references (three pages) and another seven pages for figures. This results in roughly six pages for the Introduction, Methods, Results and Discussion. That said, I do not find a good reason to avoid including relevant information that is necessary from the formal point of view. For example, the paper does not have a 'Data availability' section (mandatory in many journals) and in the lines here referred there is no information about the source for the ERA-5 or AURA-MLS data. It must be said which is the source for the data: Is it the ERA5 repository in the ECMWF? A local copy at the University of Saskatchewan or NCAR? Was the dataset retrieved through the Internet? If yes, when was it last accessed?.

Also, it would be desirable to include a Zenodo repository with the data files containing the SHOW measurements used in this work. Do not get me wrong; this information is necessary to assure independent reproducibility of the work. Therefore, I recommend the authors to take into account at least some of these recommendations. They will improve the manuscript.

We have added the following Data Availability section at the end of the paper:

Data Availability. *The ERA-5 reanalysis product was downloaded from the ECMWF online repository which can be accessed at https://cds.climate.copernicus.eu/cdsapp#!/dataset/reanalysis-era5-pressure-levels. The AURA-MLS version v4.2 data was downloaded from the GES-DISC link found at https://ml.jpl.nasa.gov/data/. The SHOW data is available upon request from the author.*

L92: ...is a spatial heterodyne

Corrected in the text

L115: Langille et al. (2019)

Corrected in the text

L121: 1 hPa to 1000 hPa

Corrected in the text

L133: Kunz et al. say that the typical PV values for the tropopause range between 1.5 and 5 PVU and in Fig. 3 the transition values highlighted are 6 and 8 PVU. Moreover, it seems hard that the transition is located along such isolines. I understand that the authors have not performed specific computations for the corresponding tropopause-PV values in this case, Right? This should be acknowledged in the text, saying that the used values are an informed guess.

Response to this comment:

One of the main findings of Kunz et al., 2011 is that based on the isentropic gradient, the PV value representing the tropopause increases with the isentropic levels. In Figure 6 of the paper, this point is shown quantitatively (see this Figure reproduced below). For the JJA season, the average tropopause PV value for the 380K is greater than 6 PVU.

This point is verified and supported by trace gas measurements-based PV tropopause. One example is shown in Kunz et al., 2011b (Figure 7 included below)

Figure 6 from Kunz et al., 2011a:

D01110 KUNZ ET AL.: TROPOPAUSE BASED ON PV GRADIENTS D01110

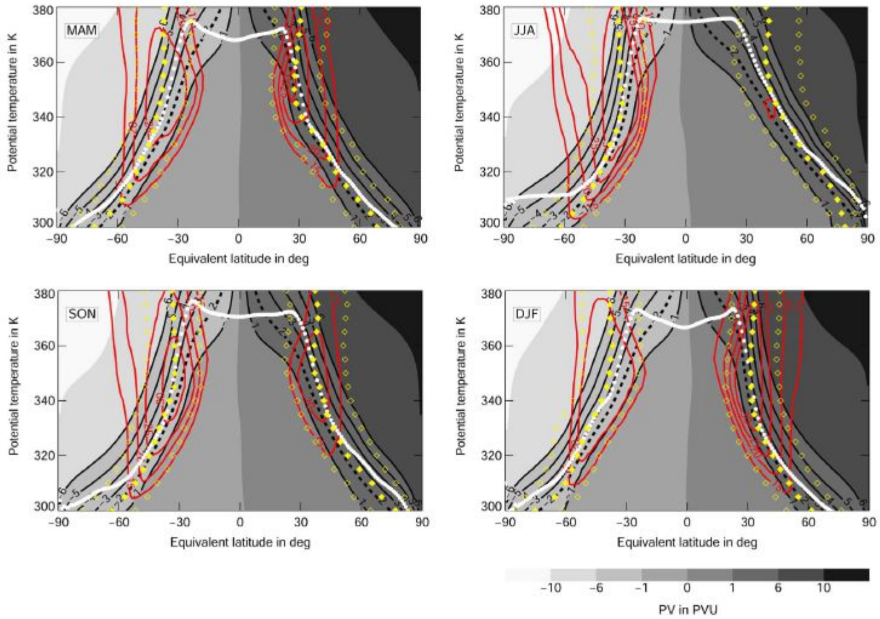

Figure 6. Zonal mean PV in PVU with equivalent latitude for different seasons in 2002. The dynamical tropopause, φ_e^{TP} (yellow diamonds), and the transition region, φ_e^{B} (open yellow diamonds), are shown on each isentrope. The height of the thermal tropopause, $\theta_{\mathrm{TP}_{\mathrm{th}}}$, is shown by white dots. Specific PV isolines between ±1 and ±6 PVU are highlighted by black solid lines. The 2 PVU isoline is a black dashed line and the zonal wind is shown in red.

Figure 7 from Kunz et al., 2011b:

D24302 KUNZ ET AL.: CHEMICAL AND

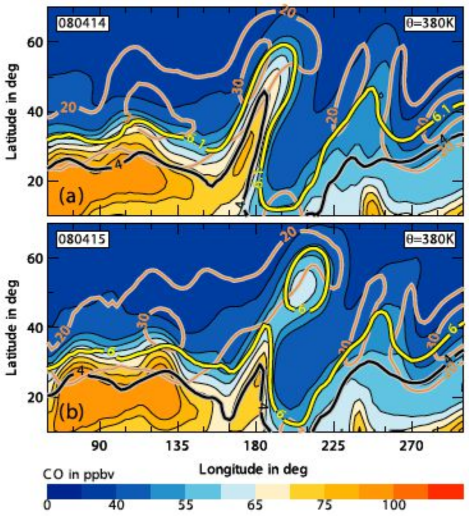

Figure 7. WACCM CO distribution at 380 K on (a) 14 April 2008 and (b) 15 April 2008. PV^{TP} is represented by the 6.1 PVU isoline on 14 April and by the 6.0 PVU isoline on 15 April 2008 (yellow line). The 4 PVU isoline (black line) and the horizontal wind speed (orange contours) are also shown.

There has not been a systematic study of PV horizontal gradient at the 400 K level. The use of 8 pvu is consistent with the increasing tendency revealed in Kunz et al. 2011 and also consistent with the observed dynamical structure.

To be more accurate without over burden the statement, we made the following revision to this sentence:

"Here, we used 6 pvu to identify the separation between tropospheric air on the 380 K surface (Kunz et al., 2011), which is noted by the white transition region between red (low PV air and tropospheric) and blue (high PV air and stratospheric) colors in the figures. Similarly, we used 8 pvu to represent this separation on the 400 K isentropic surface, which consistently highlighted the filament of tropical air (more tropospheric) in the background of extratropical (lower stratospheric) background."

References: (the first one is already in the paper. The second one is just for the referee or editor to see)

Kunz, A., P. Konopka, R. Müller, and L. L. Pan (2011a), Dynamical tropopause based on isentropic potential vorticity gradients, J. Geophys. Res., 116, D01110, doi:10.1029/2010JD014343.

Kunz, A., L.L. Pan, P. Konopka, D. E. Kinnison, and S. Tilmes (2011b), Chemical and dynamical discontinuity at the extratropical tropopause based on START08 and WACCM analyses, J. Geophys. Res., 116, D24302, doi:10.1029/2011JD016686.

L141: The WMO (1992) reference is not in the list.

Corrected in the text.

Figure 5. In the caption, 'SHOW' should be capitalized. Also, it should not appear a blank space between the degree symbol and the letter for the cardinal point.

Corrected in the text.

Figure 6. In the caption 'light grey' corresponds to PV, and zonal wind is in black.

Corrected in the text.

L244: HIRDLS

Corrected in the text

L251: PVU

Corrected in the text

L261: ' ...which is a sign of irreversible transport.'

Corrected in the text

Figures 6B and 7C: You use ERA5, so change ECMWF by ERA5 in the titles. The ECMWF has many reanalysis products, and as it is now, it is not clear enough what you mean. Readers could find it confusing.

Corrected in these figures

L327: Langille et al. (2018)

Corrected in the text

L340: 2018)

Corrected in the text

The citation style of this journal uses parenthesis, not brackets.

Corrected in the text

Additional author corrections:

Figure 6b. Figure 7b, Figure 7c: We adjusted the saturation limits so that values that are off the scale are no longer white. In Figure 7b the lower limit was also adjusted to bring out the spatial structure.

Figure 7a: The altitudes in the original Figure were calculated directly from the MLS pressure levels assuming a fixed scale height and reference pressure. The Figure has been updated with calculated altitudes from the MLS pressure levels using the relationship between the ERA5 pressure levels and the geometric height calculated from the ERA5 geopotential height. The calculation is more accurate and results in only minor changes to the Figure.

Minor corrections suggested by the Editor:

P7, L183: within in -> either "within" or "in"

Corrected in the text

P8, Figure 5 caption: colon after Figure 5 missing (this holds also for the other figures).

Corrected in the text

P8, FIgure 5 caption: show -> SHOW?

Corrected in the text

P10, L239: sits -> is located

Corrected in the text

P10, L241: has layered structure -> has a layered structure

Corrected in the text

P10, L244: HIRDLES -> HIRDLS

Corrected in the text

P10, L251: pvu -> PVU

Corrected in the text

P11, L286: degree sign is missing.

Corrected in the text

Observational evidence of moistening the lowermost stratosphere via isentropic mixing across the subtropical jet

Jeffery Langille[1], Adam Bourassa[1], Laura L. Pan[2], Daniel Letros[1], Brian Solheim[1], Doug Degenstein[1], Daniel Zawada[1]

[1]Institute of Space and Atmospheric Studies, University of Saskatchewan, Saskatoon, S7N 5E2, Canada
[2]National Center for Atmospheric Research, Boulder Colorado, 3090 Center Green Drive, CO 80301, USA

Correspondence to: Jeffery Langille (jeff.langille@usask.ca)

Abstract. Isentropic mixing across and above the subtropical jet is a significant mechanism for stratosphere-troposphere exchange. In this work, we show new observational evidence on the role of this process in moistening the lowermost stratosphere. The new measurement, obtained from the Spatial Heterodyne Observations of Water (SHOW) instrument during a demonstration flight on the NASA's ER-2 high-altitude research aircraft, captured an event of poleward water vapour transport, including a fine scale (vertically ~ < 1 km) moist filament above the local tropopause in a high spatial resolution two-dimensional cross-section of the water vapour distribution. Analysis of these measurements combined with ERA5 reanalysis data reveals that this poleward mixing of air with enhanced water vapour occurred in the region of a double tropopause following a large Rossby wave breaking event. These new observations highlight the importance of high resolution measurements in resolving processes that are important to the lowermost stratosphere water vapour budget.

1. Introduction

The distribution of water vapour in the upper troposphere and lower stratosphere (UTLS) region plays a critical role in the physical processes that couple the region to Earth's climate. This is especially true near the tropopause and in the lower stratosphere where the radiative sensitivity and climate impact of water vapour is most significant (de Forster and shine, 1999; de Forster and Shine, 2002; Solomon et al., 2010). Several studies have shown that trends in stratospheric water vapour affect long term and recent climate trends (e.g., Solomon et al., 2010; Dessler et al., 2013; Banerjee et al., 2019). Due to the strong gradient in the water vapour distribution across the tropopause and the fact that controlling mechanisms often involve small scale processes, quantifying stratospheric water vapour and its trends remains challenging for both observations and modelling (Kley et al., 2000; Gettelman et al., 2010; Riese et al., 2012; Högberg, et al., 2019; Nedoluha et al., 2017).

In this work, we present a case study of high-spatial-resolution observations of UTLS water vapour that has been enabled by new measurement technology. The measurements, using the Spatial Heterodyne Observations of Water (SHOW) instrument (Langille et al., 2018) on board the NASA ER-2 research aircraft during a demonstration flight, captured an event of water vapour transport into the lowermost stratosphere across the subtropical jet. Using ECMWF ~~ERA-5~~ERA5 reanalysis product, we demonstrate the transport is driven by a large scale Rossby-wave breaking event and in association with the occurrence of a double tropopause. Together, the result demonstrates the importance of isentropic transport processes for the stratospheric water vapour budget, and the importance of high-resolution water vapour measurements in the UTLS.

In the middle-world, the layer of atmosphere between 310 K and 380-400 K, the isentropic surfaces intersect the tropopause in the subtropics (Holton, 1995 and reference therein). A ubiquitous feature here is a sudden decrease~~drop~~ in the altitude of the thermal tropopause near the subtropical jet, known as the "tropopause break". The layer poleward of the break is defined as the lowermost stratosphere and is strongly influenced by transport via isentropic mixing associated with Rossby wave breaking (e.g., Chen, 1995; Scott and Cammas, 2002). The role of isentropic mixing in the budget of lowermost stratosphere water vapour has been highlighted by both in-situ airborne and balloon observations (e.g., Dessler et al., 1995; Hintsa et al., 1998; Ray et al., 1999) and satellite measurements (e.g., Pan et al., 1997). A number of more recent studies have shown that the occurrence of a double tropopause~~ is~~ can be associated with Rossby- wave breaking and large-scale poleward transport. Chemical signatures of this type of transport has been observed in ozone and a number of other species (Pan et al., 2009; Homeyer et al. 2011; Ungermann et al., 2013). The observation reported in this work, however, represents the first such measurement of the 2-dimensional structure of the water vapour distribution.

The~~ Spatial Heterodyne Observations of Water (~~SHOW~~)~~ instrument is a new limb sounding satellite prototype originally designed and built at York U~~u~~niversity that is being further developed in collaboration between the University of Saskatchewan and the Canadian Space Agency to provide high vertical resolution (< 250 m) measurements of water vapour with high precision (< ±1 ppm) in the UTLS region. ~~The instrument implements a limb imaging spatial heterodyne spectrometer (SHS) to obtain vertically resolved images of the water vapour spectrum using limb-scattered sunlight in a 2 nm spectral window centered on 1364.5 nm (Langille et al., 2017). Each SHOW measurement is inverted using the optimal estimation approach to obtain the vertical water vapour profile for each along-track sample (Langille et al., 2018).~~

The~~ SHOW~~ prototype version of the instrument (see Section 2) flew several demonstration flights on NASA's ER-2 airplane in July, 2017 in order to validate the measurement approach and to demonstrate the along-track sampling capabilities of the instrument. The ~~SHOW~~ measurement technique, retrieval approach and instrument performance was validated during an Engineering flight that was performed on July 17, 2017~~8~~ (Langille et al., 2019). Comparison with co-located radiosonde measurements were found to be in excellent agreement, with the radiosonde recording a positive bias of ~ 3.3% relative to SHOW and percent differences of < ±10 %~~ < 1 ppm above 15 km (near the thermal tropopause) and < 2-5 ppm below 15~~ km, due to both natural variability between the observations and measurement precision.

The analysis of this work focuses on another flight performed on July 21, 2017. The flight path (Figure 1), across several degrees of latitude off the west coast of North America from roughly 34° North to 48° North along the 124.5° West longitude line, was chosen in an attempt to observe potential mixing near the tropopause break in a region known to have a relatively frequent occurrence of double tropopauses in summer season (~~[~~Anel et al., 2008)~~]~~. This mixing process often produce fine scale filaments that are difficult for the satellite measurements and the large-scale models to resolve. The result of the measurement indeed shows fine scale water vapour structures which reveals poleward mixing of moist filaments in the region of a double tropopause, demonstrating the capability of the new measurement technology in capturing the climate relevant water vapour transport process.

Meteorological fields determined from the ECMWF ~~ERA-5~~ERA5 reanalysis are used to examine the dynamical setting of the measurements. To support the process understanding, the Rossby-wave breaking event that proceeds the observation is examined using isentropic maps of potential vorticity (PV). Also examined to support the process identification is the nearly coincident retrievals of ozone and water vapour from the AURA-MLS instrument.

2. The Spatial Heterodyne Observations of Water (SHOW) instrument

The SHOW instrument is a spatial heterodyne spectrometer that has been optimized for limb viewing observations of limb-scattered sunlight within a vibrational band of water. The limb is imaged conjugate to the SHS interference fringes such that each interferogram row and subsequently each spectral row in the image is mapped one-to-one to line of sight at the limb. Each sample provides a vertically resolved spectral image with ~0.03 nm spectral resolution in a 2 nm window centered on 1364.5 nm. These vertically resolved spectral images are inverted using a non-linear optimal estimation approach to obtain the vertical distribution of water vapour. The SHOW measurement technique and retrieval algorithm is discussed in previous publications (~~[~~Langille et al., 2018; Langille et al., 2019)~~]~~.

Instrument parameter	Specification
ER-2 airplane altitude	**~21.34 km (70000 ft max)**
Airplane speed	**~760 km/h (maximum at altitude)**
Field Of View	**4° vertical by 5.1° horizontal**
Temporal cadence	**1Hz or 0.5 Hz**
Spatial sampling at the surface	**~1 km @ 1 Hz**
Instantaneous angular vertical resolution	**0.0176 degrees**
Retrieval altitudes	**13 km to 18 km**
Retrieval grid	**250 m**
Mass	**222.68 lbs [101 kg]**
Power	**465 W (peak), 200 W (average)**
Dimensions	**(0.465 m × 1.32 m× 0.38 m)**
Spectral Resolution (unapodized)	**~0.03 nm**
Spectral range	**1363 nm – 1366 nm**

Table 1: SHOW ER-2 instrument parameters

The prototype SHOW instrument is optimized for observations from NASA's ER-2 airplane and is mounted in a forward looking wing pod to observe a 4 degree vertical by 5.1 degree horizontal field of view. Flying at an altitude of 21 km, the viewing geometry and optical configuration provides a vertical sampling at the limb tangent point of 51 m to 171 m, increasing towards the ground tangent. The instrument utilizes anamorphic optics to average over the scene in the horizontal dimension; therefore, no horizontal (longitudinal) scene information is obtained. Using this configuration, retrievals are performed on a 250 m retrieval grid with no smoothing to provide an approximate vertical resolution of 250 m from 13 km up to 18 km with precisions better than 1 ppm. The instrument can be operated using sampling rates from 0.1 Hz up to 2 Hz mode; however, the measurements discussed in this paper are obtained using a sampling rate of 1Hz. This provides an approximate raw along track sampling of ~0.5 km at the surface (or ~0.005 degrees latitude). The primary instrument specifications are listed in Table 1 and the full instrument configuration is presented in Langille et al.~~,~~ (2019).

3. ER-2 flight track and the metrological background

The measurements discussed in this paper were obtained during a flight on board the ER-2 performed on July 21, 2017 between 18:00 UTC and 19:00 UTC off the Western coast of North America. For analysis of the meteorological fields within this measurement window we utilize the ECMWF (~~ERA-5~~ERA5) reanalysis products, which are provided in 1-hour time steps on a 0.25 degree x 0.25 degree grid (latitude x longitude) at 37 pressure levels from 1 hPa~~mbar~~ up to 1000 hPa~~mbar~~.

To provide the dynamical background of the flight track, the zonal wind at the 175-hPa level (approximately 13 km altitude) for the 18:00:00 UTC time step on July 21, 2017 is shown in Figure 1. The zonal wind field shows a double jet structure with the subtropical jet located near 35˚ North and the polar jet near 45°North. Both features have jet cores (with winds > 40 m/s) that are located over the Pacific Ocean. As the subtropical jet is shifting north, downstream in an anticyclonic flow, the two jets merge over North America. This configuration is formed with a large-scale Rossby wave-breaking event that developed over several days prior to the SHOW ~~measurements, and~~measurements and is demonstrated in Figure 2 using the 380 K isentropic potential vorticity in 48-hour intervals over a six days period. To further connect with the ER-2 track, the potential vorticity on the 380 K and 400 K surfaces is shown in Figure 3 for the 21/07/2017 time step. Here, we used 6 PVU to identify the separation between tropospheric air on the 380 K surface (Kunz et al., 2011), which is noted by the white transition region between red (low PV air and tropospheric) and blue (high PV air and stratospheric) colors in the figure. A well-defined low PV structure consistent with tropospheric air is observed on the 380 K surface that extends from the Western Pacific up to the extratropical region over North America as a result of the wave breaking. Similarly, we used 8 PVU to represent this separation on the 400 K isentropic surface, which consistently highlighted the filament of tropical air (more tropospheric) in the background of extratropical (lower stratospheric) background. ~~Here, the separation between stratospheric and tropospheric air occurs near 6 PVU and 8 PVU, respectively (Kunz et al., 2011), which is the noted by the white transition region between red (low PV air and tropospheric) and blue (high PV air and stratospheric) colors in the figures.~~ ~~A well-defined low PV structure consistent with tropospheric air is observed on the 380 K surface that extends from the Western Pacific up to the extratropical region over North America as a result of the wave breaking.~~

To characterize the dynamical structure vertically, the height of the thermal tropopause and the occurrence of the double tropopause is shown in Figure 4. Here the tropopause is derived using the ~~ERA-5~~ERA5 temperature field using the lapse rate definition (WMO, 1957; 1992) with a modification. The modified version locates the first tropopause as the lowest level where the lapse rate drops below 2 K/km and remains below that value on average for 1 km (instead of 2 km). A second tropopause is identified if the lapse rate increases above 2K/ km (instead of 3 K/km) and then decreases again below 2 K/km. This is done to remedy the coarse vertical resolution of the of the temperature data. This type of modification has been recognized to allow identification of the double tropopause derived from coarse resolution temperature data that is more consistent with high resolution observational data (Randel et al., 2007). ~~In particular, our~~Our goal here is to highlight the spatial extent of the layered static stability structure as discussed in Sections 4-5. The height distribution of the primary tropopause is shown in Figure 4 (a). The distribution of the secondary tropopause, shown in Figure 4 (b), is consistent with the formation mechanism of a poleward wave breaking along the subtropical jet (Pan et al., 2009). Although not shown here, the double tropopause features have varying strength from time-step to time- step on the days leading up to and after the flight. Occurrences of double tropopauses are common in this region with the highest occurrence rate in the winter (~~[~~Swartz et al., 2014)~~]~~; although, they are also observed in the summer season (~~[~~Anel et al., 2008)~~]~~.

The ER-2 flight track with the SHOW instrument for the 18:00 UTC to 19:00 UTC time period, as indicated in Figures 1, 3 and 4, includes the edge of a large double tropopause region that extends off the Western coast of the United States. For process verification using an independent measurement, we identified a near co-located MLS satellite observation track, also marked on Figures 1, 3, and 4. Analysis of the SHOW and MLS measurements are discussed in Section 4 and Section 5 respectively.

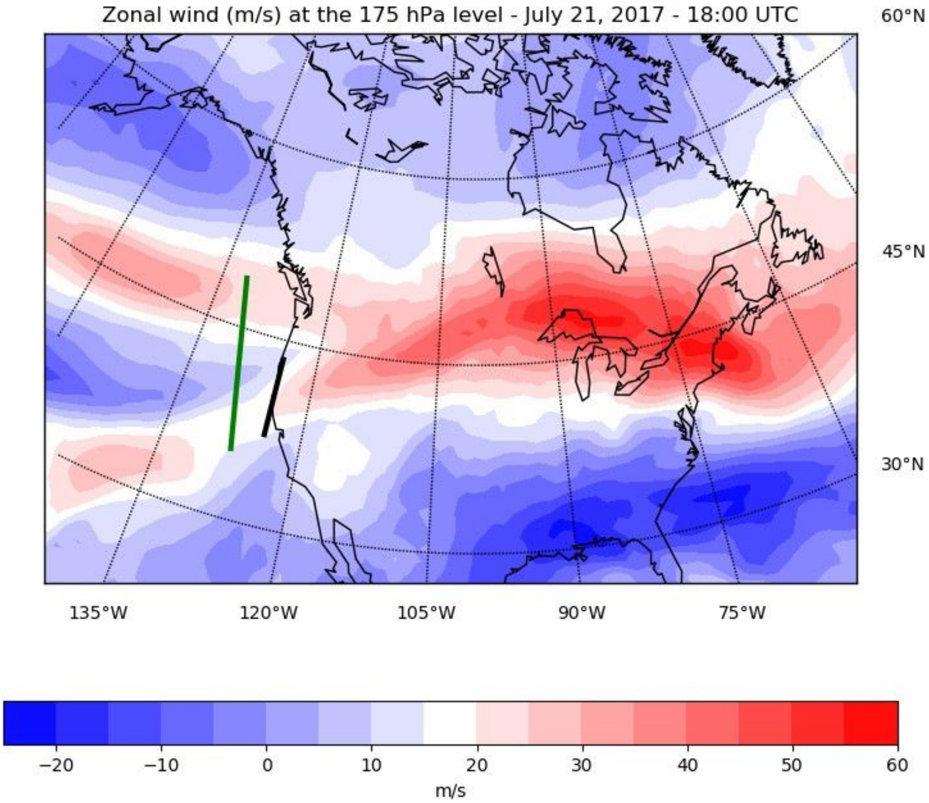
Zonal wind (m/s) at the 175 hPa level - July 21, 2017 - 18:00 UTC
60°N
45°N
30°N
135°W
120°W
105°W
90°W
75°W
−20
−10
0
10
20
30
40
50
60
m/s

Figure 1: Zonal wind on the 175 hPa surface for the 18:00 UTC, July 21, 2017~~9~~ time step. The ER-2 flight track with the SHOW measurements is shown as the black line and the closest measurement track of the AURA-MLS instrument is shown as the dark green line.

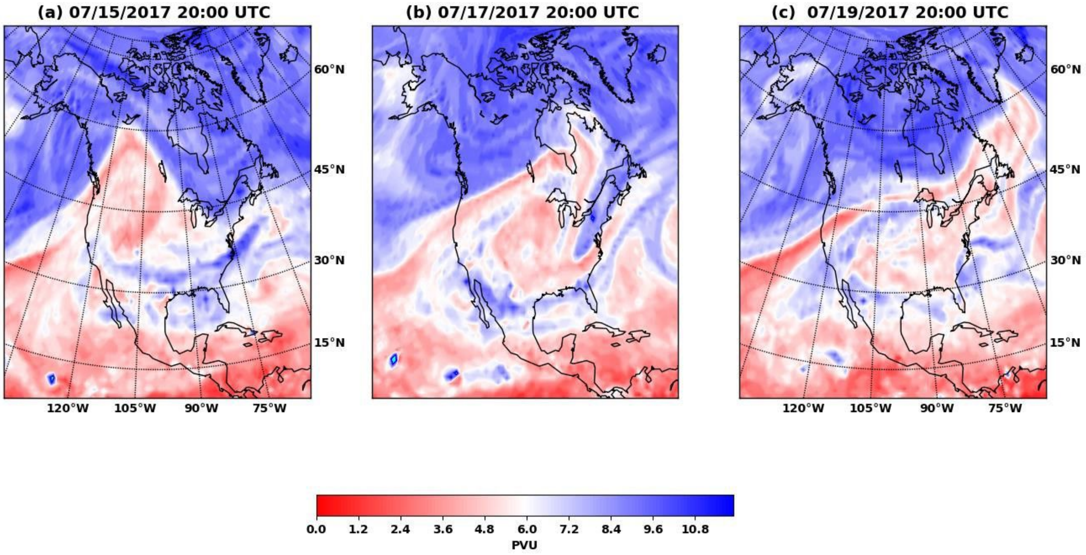

Figure 2: Potential vorticity on the 380 K isentropic surface on 07/15/2017, 07/17/2017 an 07/19/2017 at 20:00 UTC showing a Rossby wave breaking event several days prior to the SHOW measurements.

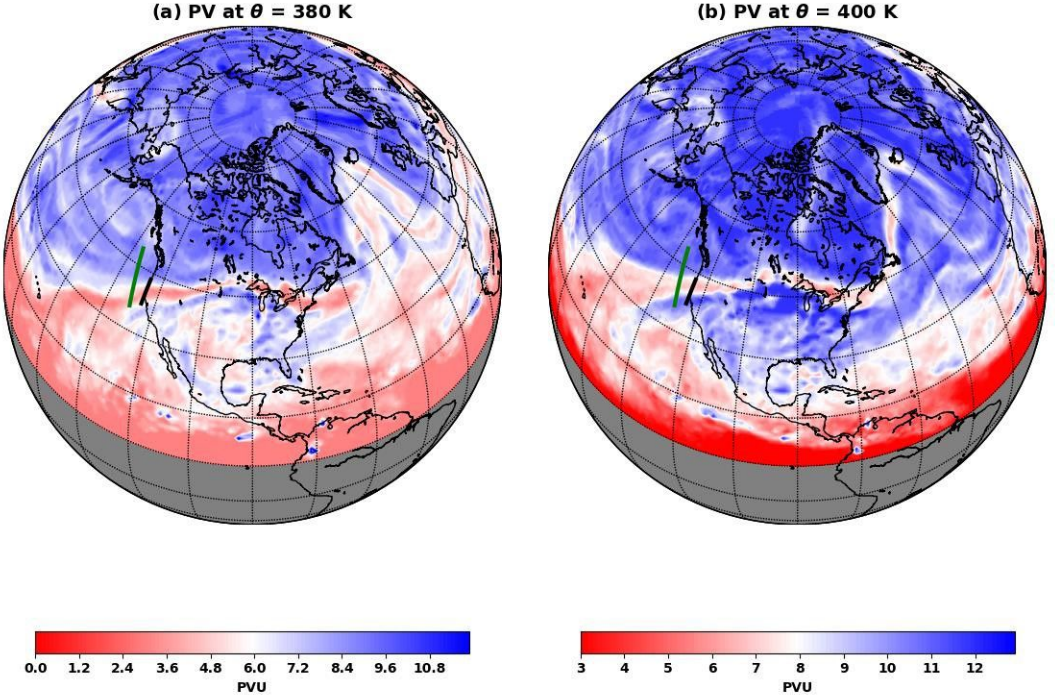

Figure 3: Potential vorticity on the 380 K (a) and 400 K (b) isentropic surfaces for the 18:00 UTC, July 21, 2017~~9~~ time step. The measurement track of SHOW and MLS are shown in black and green respectively.

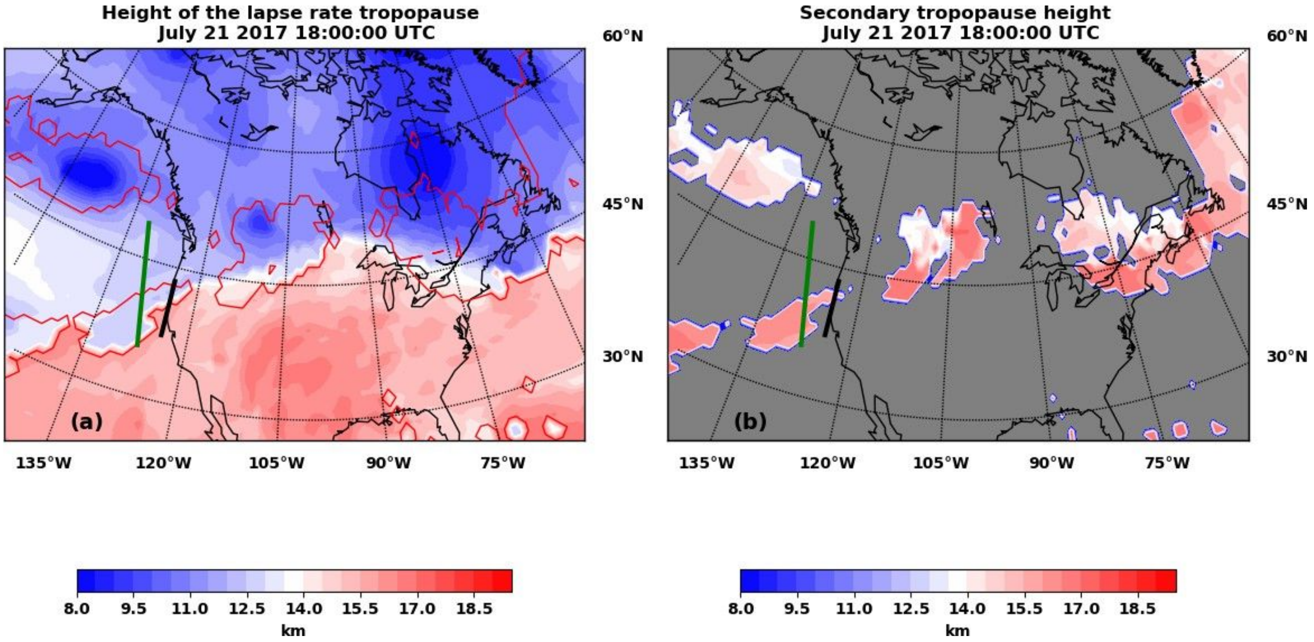

Figure 4: Height of the thermal tropopause (a) and the height of the secondary tropopause (b) for the 18:00 UTC time step. The red outline in (a) denotes the edge of the double tropopause regions shown in (b). The measurement track of SHOW and MLS are shown in black and green respectively.

4. SHOW Observations

We begin the analysis of SHOW water vapour measurements with three example profiles, shown in Figure 5 (a-c), which correspond to the latitude bins centered at 37.4 degrees North ~~profiles~~, 41.87 degrees North and 43.48 degrees North respectively. Each example shows the set of 10 samples obtained within ~~in~~ each latitude bin (black) and the mean of the sample set (red). The observed variance in the water vapour distribution closely matches the 1-2 ppm measurement error predicted by propagating the noise through the retrieval. The red error bars show the precision for the averaged measurements which is less than < 0.3 ppm for most measurement altitudes. The upper and lower boundaries of the retrievals presented in this paper are 18 km and 13.5 km respectively. The altitude of the first and second lapse rate tropopause are shown as blue solid and dashed lines respectively.

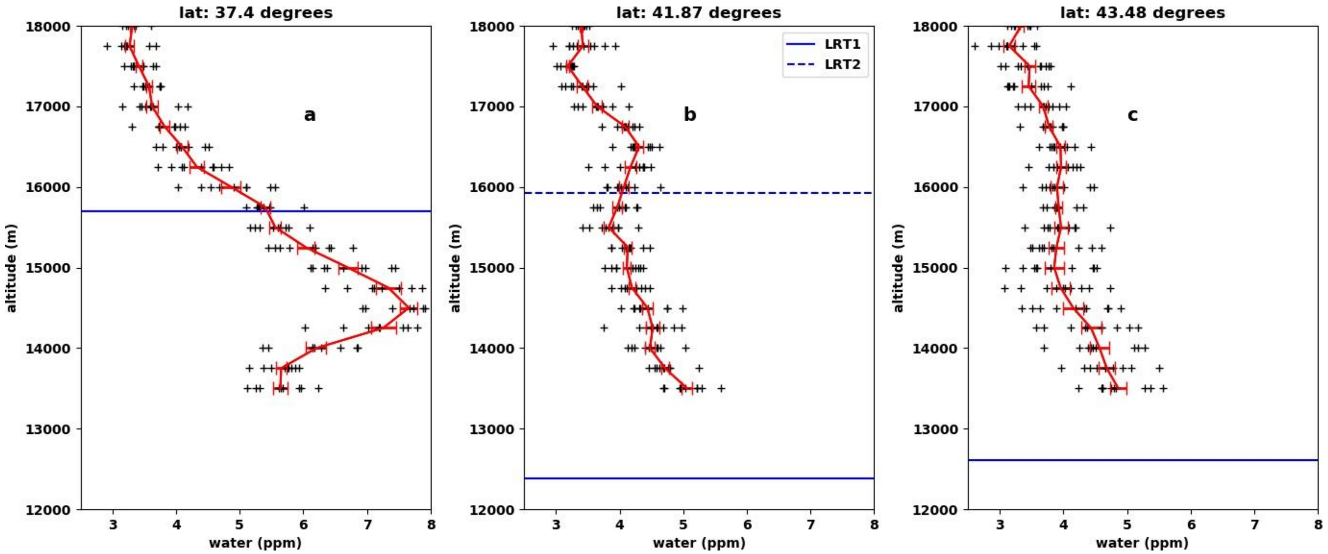

Figure 5: Example SHOW~~show~~ profiles at 37.4° N (a), 41.87° N (b), and 43.48° N (c). All profiles lie closely along~~ the~~ the 124.5° W ~~in~~ longitude line. The black data points correspond to each of the individual profiles and the red line is the average of all latitude measurements in each altitude bin. The error bars show the precision of the averaged measurements. The first and second tropopause are identified in the Figure with the solid blue and dotted blue lines respectively.

For the 37.4° N measurement, the water vapour mixing ratio increases to a maximum near 14.5 km and then decreases rapidly with increasing altitude. The water vapour mixing ratio is also found to decrease slightly below 14.6 km. In the current analysis, the lower boundary of the retrieval is at 13.5 km and therefore doesn’t capture the expected increase of water vapour at altitudes below 13.5 km. At 41.87° N a secondary peak in the water vapour profile is observed near 16.5 km. The amount of water vapour decreases slightly below this peak and then continues to steadily increase with decreasing altitude. Further along the flight track, at 43.48° N, the peak at 16.5 km has diminished and the amount of water vapour increases slowly with decreasing altitude.

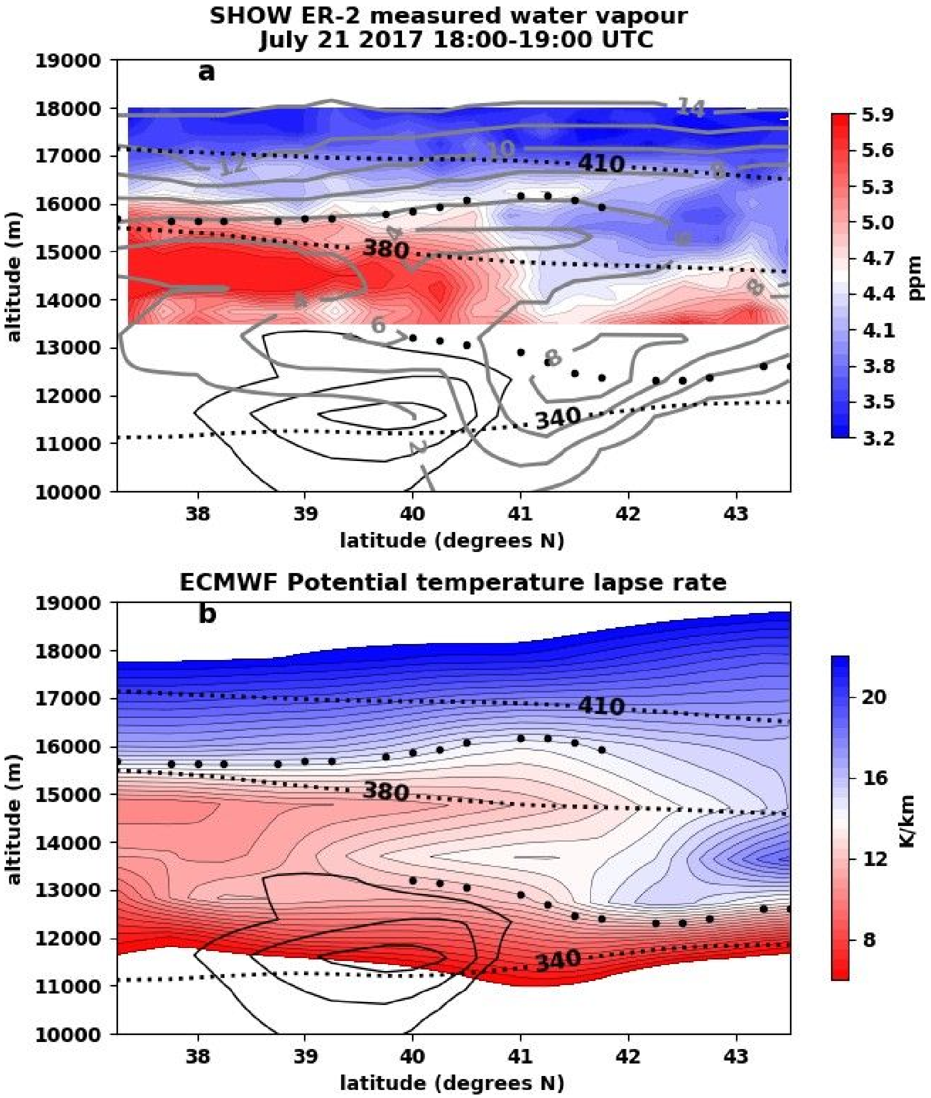
SHOW ER-2 measured water vapour
July 21 2017 18:00-19:00 UTC
a
altitude (m)
19000
18000
17000
16000
15000
14000
13000
12000
11000
10000
14
10
12
410
8
4
380
6
4
8
6
8
340
2
38
39
40
41
42
43
latitude (degrees N)
5.9
5.6
5.3
5.0
4.7
4.4
4.1
3.8
3.5
3.2
ppm
ECMWF Potential temperature lapse rate
b
altitude (m)
19000
18000
17000
16000
15000
14000
13000
12000
11000
10000
410
380
340
38
39
40
41
42
43
latitude (degrees N)
20
16
12
8
K/km

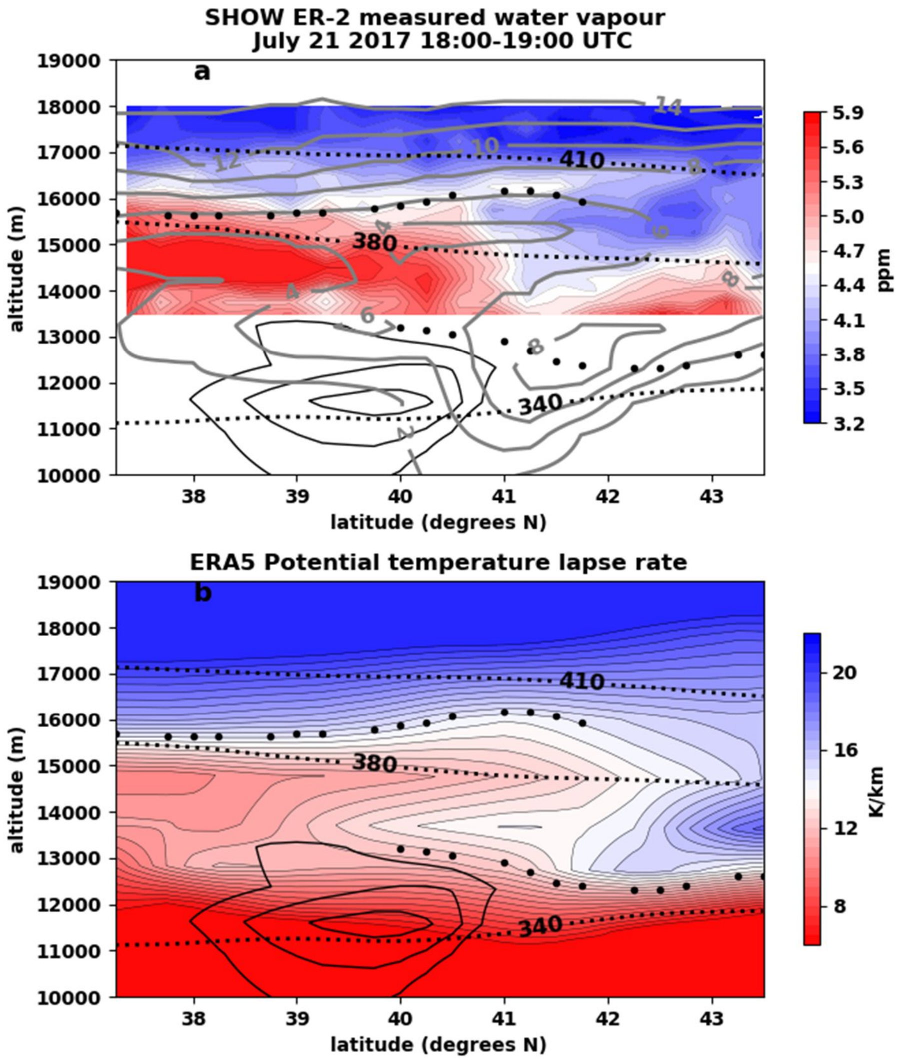

Figure 6: SHOW measured water vapour profile (from 18:00 UTC to 19:00 UTC) (a) and the potential temperature lapse rate determined from the ERA5 ~~ECMWF~~ reanalysis for the 19:00 UTC time step along the SHOW measurement track (b). The dark dotted line shows the location of the thermal tropopause. The grey contours show the potential vorticity, several zonal wind contours are shown in black~~light grey~~, and the light black dotted line shows the 340 K, 380 K and 410 K isentropes respectively. The longitude is along the 124.5° W line and is nearly constant for the measurements.

All of the measured water vapour profiles obtained along the flight track are stacked and plotted as a single data curtain in Figure 6 (a). Along this track, SHOW obtained high vertical resolution (< 250 m) measurements of UTLS water vapour around the tropopause (13 km – 18 km). These measurements were then averaged by latitude to increase the signal to noise ratio, resulting in an along track sampling of approximately 0.32 degrees latitude~~ (approximately 36 km at the ground)~~. The result provides a high vertical resolution time (latitude) – height cross-section of the water vapour distribution along the flight track. The dynamical fields, including zonal wind~~, potential temperature~~, potential vorticity and the derived tropopause locations from the ECMWF ERA5 reanalysis (18:00 UTC time step) are overlaid on top of the water vapour measurements. The dynamical structure in the cross-section co-located with the flight track is further examined in Figure 6 (b), where the structure of the static stability is highlighted using the potential temperature lapse rate determined from the reanalysis data ($PTLR = {}^{\Delta\theta}/_{\Delta z}$). In both figures, the 340 K, 380 K and 410 K isentropes are shown as the thin dotted lines and the thick black dots identify the location of the thermal tropopause.

The 410 K isentrope lies entirely in the stratosphere (in the overworld) at all latitudes. Above the 410 K isentrope, the water vapour mixing ratio is observed to have values between 3.0 ppm – 4.0 ppm which defines the background water vapour mixing ratio in the lowermost stratosphere. Near the tropopause (in the middleworld), sharp spatial structures are resolved that have gradients on the order of 0.5 ppm per 250 m sampling bin. SHOW does not record the water vapour distribution below the 340 K isentrope since the retrieval cuts off at an altitude of 13.5 km. Discussion of this lower boundary is presented in Section 6.

The dynamical structure of the cross-section identifies the flight track extended over a well-defined tropopause break over the jet core, which is indicated by tight zonal wind contours (black) near 39.9° latitude. South of 39.9° latitude, the thermal tropopause ~~sits~~ is located at an altitude of close to 15.5 km. The region of 39.9° to 42° has a double tropopause structure. More importantly, the region of the tropopause break has a layered structure of static stability, showing a layer of low stability, tropospheric like air mass extending poleward over the primary tropopause. Consistent with the stability structure, the PV field (grey) in the region shows weakened gradient. Overall, the dynamical background has a large similarity with the observed tropospheric intrusion from the HIRDL~~E~~S satellite ozone case study (Fig. 1 in Pan et al., 2009).

Water vapour measurements from SHOW (Figure 6 a) recorded a layer with water vapour mixing ratio greater than 5 ppmv which is much higher than the stratospheric background, centered at roughly 14.6 km, and extends poleward to about 40.5° above the local primary tropopause. Note that the layer in between the two tropopauses where the PV distribution shows a weakened gradient between the 4 and 8 PVU~~pvu~~ contours, indicating a weakened tropopause (Pan et al., 2009; Kunz et al., 2011a; 2011b). Further poleward, the SHOW measurements captured ~~a~~ part of a layer with enhanced water vapour above the primary tropopause between 41.5°N and 43.5° N. The moist layer is also co-located with the weakened PV gradient.

While the static stability structure of the cross section (Fig 6b) indicates a case of intrusion of low static stability air from the subtropical troposphere into the mid-latitude lowermost stratosphere, the quasi-isentropic transport indicated by the SHOW water vapour cross-section is not entirely matching the stability structure. Considering that the observation is made in the advent of the Rossby wave breaking event, it is physically reasonable that the dynamical field and chemical structure are no longer intact, which is a sign of ~~an~~ irreversible transport. It is also likely due to the ERA5 products available to the analysis are given in much coarser vertical resolution compared to the SHOW measurements. The important point is that there is a clear process identification supported by both the water vapour measurement and the dynamical field analysis. We will see a similar shift in the analysis of the MLS water vapour and ozone data in the following section.

5. AURA MLS ozone and water vapour

For process verification, we examine measurements of water vapour and ozone that were obtained along a nearly coincident measurement track as shown in Figure 1 (solid green line). The AURA-MLS satellite instrument obtained measurements along this track at approximately 21:50~~1~~ UTC - roughly 2 hours after the SHOW measurements were performed. Along this track, the MLS instrument sampled the same geophysical feature along a slightly different path with a horizontal resolution~~n along track sampling~~ of 168 - 230 km and a vertical resolution of 1.3-3.2 km in the UTLS (316 hPa - 46 hPa). The MLS measurements have a coarser spatial resolution and the sampling is not exactly coincident with SHOW. Therefore, some differences are expected between the measurements. However, both sensors sample nearly the same region in the vicinity of the subtropical jet. Therefore, the MLS measurements are used to check for consistency with the meteorological picture in comparison with the SHOW measurements.

The AURA-MLS measurements of water vapour and ozone are shown in Figure 7 (a) and Figure 7 (b) respectively. The corresponding PTLR plot is shown in Figure 7 (c). For this comparison we use the 22:00 UTC time step of the ECMWF ~~ERA5~~ERA5 reanalysis since it is the closest available time step to the MLS measurements which occurred at close to 21:50 UTC.

The distributions of the two trace species have a spatial structure that matches the general shape of the structure observed in the PTLR plot and PV contours. As expected, the vertical distributions of the trace species are basically inverted, with water vapour decreasing with increasing altitude and vice versa for ozone. Most importantly, a filamentary structure is observed that extends from 36° N to 42° N near 16 km and coincides with the presence of a double tropopause. Again, the feature matches a similar structure that is observed in the corresponding PTLR plot and PV contours at a lower altitude (~ 15 km).

Taking the sharpest gradient in the PTLR to define the boundary between tropospheric and stratospheric air we see that tropospheric air is primarily characterized with a PTLR < 12 K/km and stratospheric air is characterized with a PTLR > 12 K/km. Therefore, as was the case with the SHOW measurements, the observed filamentary structure with PTLR < 12 K/km is consistent with the intrusion of a low static stability air from the subtropical troposphere into the mid-latitude lower stratosphere. Mixing on the poleward side of the subtropical jet results in moistening and diminished ozone in the lowermost stratosphere.

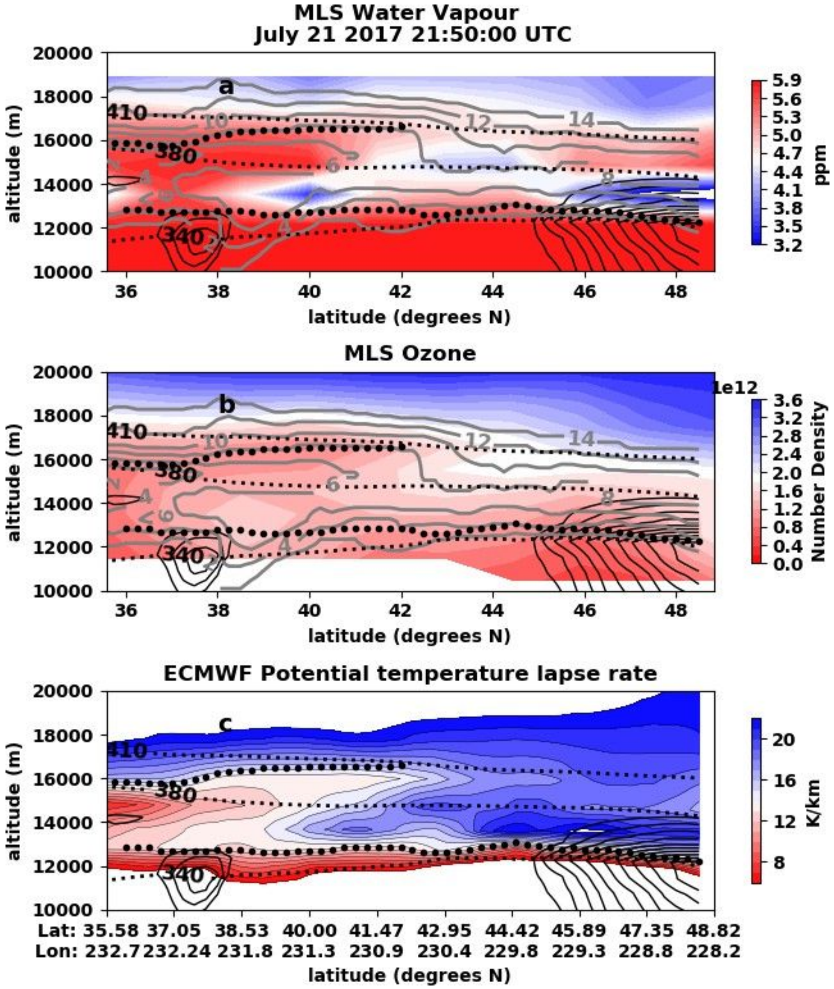
MLS Water Vapour
July 21 2017 21:50:00 UTC
a
altitude (m)
latitude (degrees N)
ppm
5.9
5.6
5.3
5.0
4.7
4.4
4.1
3.8
3.5
3.2
410
380
340
10
12
14
6
8
4
MLS Ozone
b
1e12
Number Density
3.6
3.2
2.8
2.4
2.0
1.6
1.2
0.8
0.4
0.0
ECMWF Potential temperature lapse rate
c
K/km
20
16
12
8
Lat: 35.58 37.05 38.53 40.00 41.47 42.95 44.42 45.89 47.35 48.82
Lon: 232.7 232.24 231.8 231.3 230.9 230.4 229.8 229.3 228.8 228.2
20000
18000
16000
14000
12000
10000
36
38
40
42
44
46
48

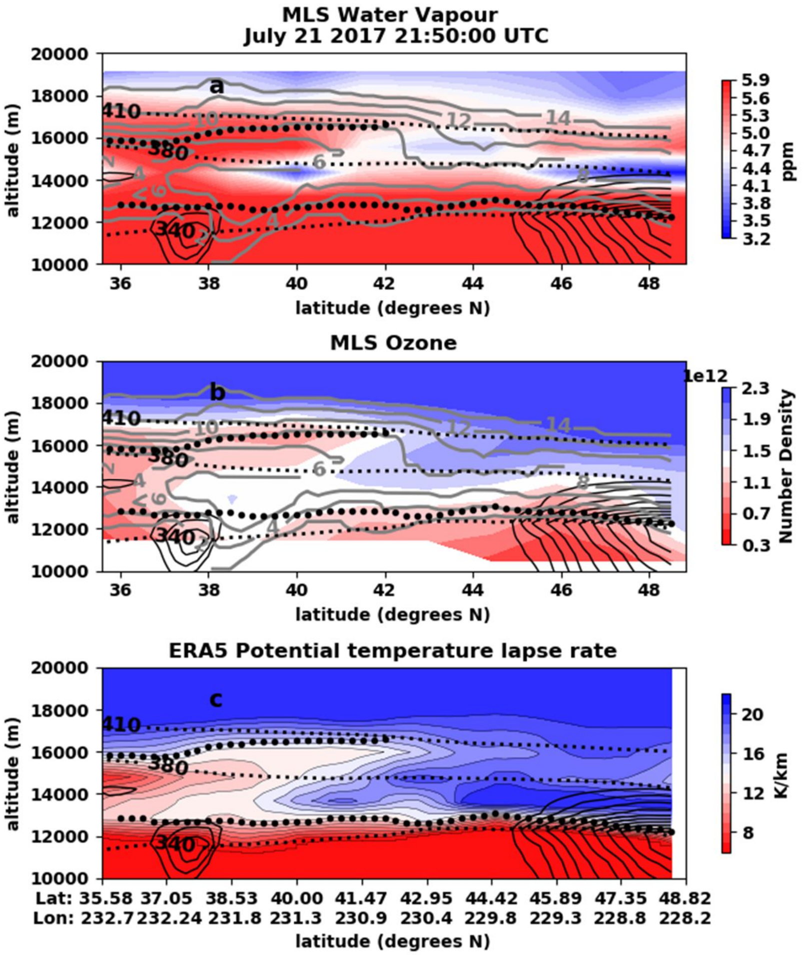

Figure 7: MLS measured water vapour profile (a), ozone (b) and the potential temperature lapse rate determined from the ~~ECMWF~~ERA5 reanalysis for the 22:00 UTC time step along the MLS measurement track (c).

The spatial structures recorded by SHOW (Figure 6) and MLS (Figure 7) during this event are strikingly similar and are consistent with spatial structures in the meteorological fields. A direct comparison shows that both instruments recorded similar amounts of water vapour in the vicinity of the subtropical jet. They both capture the moist filament near 16 km, as well as, the dry regions near 14~~13.5~~ km in the lower latitude portion of the measurement tracks. However, the coarser vertical resolution of MLS smears the vertical extent of the moist filament across a large vertical range of ~2 km.

Interestingly, the spatial structures observed in the MLS ozone and water vapour profiles are both shifted to a higher altitude relative to the PTLR and PV structures. Regardless, it is clear that the spatial variability observed in the MLS ozone and water vapour measurements, in light of the higher resolution

SHOW observations, is consistent with isentropic mixing on the poleward side of the subtropical jet in the presence of a double tropopause.

6. Discussions and Conclusions

The SHOW measurements presented in this paper reveal fine spatial structures with vertical scales < 1 km in the two-dimensional water vapour profile near the subtropical jet. The meteorological picture that was presented in Section 2 indicates that these structures are associated with isentropic transport and mixing due to the “stirring” of a Rossby wave breaking event in the days leading up to the flight. The high vertical resolution measurements of the two-dimensional water vapour distribution provide a detailed window into the mixing processes that is not completely resolved in the reanalysis dynamical fields or the AURA MLS measurements.

The vertical resolution of the measurements determined from the full-width half maximum of the retrieval averaging kernel is 250 m and the precision on the measurements is < 0.3 ppm. The accuracy of the SHOW measurements and retrieval approach was examined in Langille et al.~~,~~ (2018) and was found to be < 0.5 ppm for a wide range of water vapour variability and background aerosol. The approximate line-of-sight accuracy of the SHOW observations determined from the flight data is < 150 m in the 13 km -18 km region. Comparison with collocated radiosonde measurements obtained during an Engineering flight on July 17, 2019 also showed excellent agreement (~~[~~Langille et al., 2019)~~]~~. This provides reasonable level of confidence that the variability observed in Figure 6 is reflective of the true state of the atmosphere at the time of measurement.

However, we must also note that the SHOW retrieved profile~~al~~ is sensitive to the upper and lower cut-off of the retrieval. In this paper, the upper boundary was chosen to be roughly 2 km below the aircraft altitude. Above this level, the sensitivity to water vapour is significantly reduced as the path between the aircraft and tangent point decreases. On the other hand, the lower boundary was chosen to be several km below the lapse rate tropopause at the beginning of the measurements. Below this level, the optical depth becomes too large to accurately retrieve water vapour information (~~[~~see Langille et al., 2018). Ideally, this lower cutoff would be actively chosen to track changes in the altitude of the lapse rate tropopause and allow retrievals several km below this altitude; however, the retrieval run was performed without a- priori knowledge of the meteorological picture. An active determination is also under development that utilizes the sensitivity of the Jacobian to changes in the water vapour profile to determine the appropriate cut-off (~~[~~Langille et al., 2018)~~]~~. In this paper, the lower boundary cut-off was fixed at ~~13.5 km~~13.5 km using knowledge obtained from simulated retrievals in order to ensure the retrieval was not influenced by this effect.

The objective of the comparisons with the reanalysis data, as well as AURA MLS observations, is to identify the dynamical process that produced the measured water vapour structure. A number of factors can contribute to the differences and the offset displayed in the comparison. The reanalysis data has a vertical resolution of 1-3 km in the UTLS region. Therefore, the reanalysis data set has been used to confirm that the observed variability is consistent with general meteorological picture and isentropic mixing associated with Rossby wave breaking near the subtropical jet. On the other hand, the MLS measurements provide a means to confirm consistency with the large scale spatial variability; although, the measurements are not expected to have exact agreement since the MLS measurements are made along a flight track that samples a slightly different region of the atmosphere. Also, the limb viewing geometry from a satellite is different from the aircraft and the AURA MLS measurements have a lower vertical resolution (1.3-3.2 km) compared to the SHOW measurements (250 m). The overall consistency supports the process identification despite the specific difference.

In conclusion, the high-spatial resolution measurements of a two-dimensional structure of the water vapour transport above and poleward of the subtropical jet provide unprecedented details of isentropic mixing across the tropopause break driven by Rossby wave breaking. The observed ~~significant~~ enhancement of water vapour in the lowermost stratosphere indicates that this type of transport is a significant process for the stratospheric water vapour budget. The fine structure of the water vapour in the mixing process supports the importance of the high-resolution water vapour measurement capability. These measurements also serve to demonstrate the capabilities of the SHOW instrument and further advance the technical readiness of the instrument for future satellite deployment.

Data Availability. *The ERA5 reanalysis product was downloaded from the ECMWF online repository which can be accessed at https://cds.climate.copernicus.eu/cdsapp#!/dataset/reanalysis-era5-pressure-levels. The AURA-MLS version v4.2 data was downloaded from the GES-DISC link found at https://ml.jpl.nasa.gov/data/. SHOW data utilized in this paper is available upon request from the author.*

Conflict of interest. *The authors declare that they have no conflict of interest.*

Acknowledgments. *We would like to thank the Canadian Space Agency for providing funding and support for this project.*

7. References

1 Añel, J. A., Antuña, J. C., De La Torre, L., Castanheira, J. M. and Gimeno, L.: Climatological features of global multiple tropopause events, J. Geophys. Res. Atmos., doi:10.1029/2007JD009697, 2008.

2 Banerjee, A., Chiodo, G., Previdi, M., Ponater, M., Conley, A. J. and Polvani, L. M.: Stratospheric water vapour: an important climate feedback, Clim. Dyn., doi:10.1007/s00382-019-04721-4, 2019.

3 Chen, P.: Isentropic cross-tropopause mass exchange in the extratropics, J. Geophys. Res., doi:10.1029/95jd01264, 1995.

4 Dessler, A. E., Hintsa, E. J., Weinstock, E. M., Anderson, J. G. and Chan, K. R.: Mechanisms controlling water vapour in the lower stratosphere: “A tale of two stratospheres,” J. Geophys. Res. Atmos., 100(D11), 23167–23172, doi:10.1029/95JD02455, 1995.

5 Dessler, A. E., Schoeberl, M. R., Wang, T., Davis, S. M. and Rosenlof, K. H.: Stratospheric water vapour feedback, Proc. Natl. Acad. Sci. U. S. A., doi:10.1073/pnas.1310344110, 2013.

6 Forster, P. M. de F. and Shine, K. P.: Assessing the climate impact of trends in stratospheric water vapour, Geophys. Res. Lett., doi:10.1029/2001gl013909, 2002.

7 Forster, P. M. D. F. and Shine, K. P.: Stratospheric water vapour changes as a possible contributor to observed stratospheric cooling, Geophys. Res. Lett., doi:10.1029/1999GL010487, 1999.

8 Gettelman, A., Hegglin, M. I., Son, S. W., Kim, J., Fujiwara, M., Birner, T., Kremser, S., Rex, M., Añel, J. A., Akiyoshi, H., Austin, J., Bekki, S., Braesike, P., Brhl, C., Butchart, N., Chipperfield, M., Dameris, M., Dhomse, S., Garny, H., Hardiman, S. C., Jöckel, P., Kinnison, D. E., Lamarque, J. F., Mancini, E., Marchand, M., Michou, M., Morgenstern, O., Pawson, S., Pitari, G., Plummer, D., Pyle, J. A., Rozanov, E., Scinocca, J., Shepherd, T. G., Shibata, K., Smale, D., Teyssdre, H. and Tian, W.: Multimodel assessment of the upper troposphere and lower stratosphere: Tropics and global trends, J. Geophys. Res. Atmos., doi:10.1029/2009JD013638, 2010.

9 Hintsa, E. J., Boering, K. A., Weinstock, E. M., Anderson, J. G., Gary, B. L., Pfister, L., Daube, B. C., Wofsy, S. C., Loewenstein, M., Podolske, J. R., Margitan, J. J. and Bui, T. P.: Troposphere-to-stratosphere transport in the lowermost stratosphere from measurements of H2O, CO2, N2O and O3, Geophys. Res. Lett., doi:10.1029/98GL01797, 1998.

10 Högberg, C., Lossow, S., Khosrawi, F., Bauer, R., Walker, K. A., Eriksson, P., Murtagh, D. P., Stiller, G. P., Steinwagner, J. and Zhang, Q.: The SPARC water vapour assessment II: Profile-to-profile and climatological comparisons of stratospheric δd(H2O) observations from satellite, Atmos. Chem. Phys., doi:10.5194/acp-19-2497-2019, 2019.

11 Holton, J. R., Haynes, P. H., McIntyre, M. E., Douglass, A. R., Rood, R. B. and Pfister, L.: Stratosphere-troposphere exchange, Rev. Geophys., doi:10.1029/95RG02097, 1995.

12 Homeyer, C. R., Bowman, K. P., Pan, L. L., Atlas, E. L., Gao, R. S. and Campos, T. L.: Dynamical and chemical characteristics of tropospheric intrusions observed during START08, J. Geophys. Res. Atmos., doi:10.1029/2010JD015098, 2011.

13 Kley, D., et al. (2000), SPARC assessment of upper tropospheric and stratospheric water vapour, WCRP 113,World Meteorol. Organ., Geneva, Switz.

14 Kunz, A., Konopka, P., Müller, R. and Pan, L. L.: Dynamical tropopause based on isentropic potential vorticity gradients, J. Geophys. Res., 116(D1), D01110, doi:10.1029/2010JD014343, 2011.

15 Kunz, A., Pan, L. L., Konopka, P., Kinnison, D. E. and Tilmes, S.: Chemical and dynamical discontinuity at the extratropical tropopause based on START08 and WACCM analyses, J. Geophys. Res. Atmos., 116(D24), n/a-n/a, doi:10.1029/2011JD016686, 2011.

16 Langille, J. A., Letros, D., Zawada, D., Bourassa, A., Degenstein, D. and Solheim, B.: Spatial Heterodyne Observations of Water (SHOW) vapour in the upper troposphere and lower stratosphere from a high altitude aircraft: Modelling and sensitivity analysis, J. Quant. Spectrosc. Radiat. Transf., 209, 137–149, doi:10.1016/j.jqsrt.2018.01.026, 2018.

17 Langille, J. A., Solheim, B., Bourassa, A., Degenstein, D., Brown, S. and Shepherd, G. G.: Measurement of water vapour using an imaging field-widened spatial heterodyne spectrometer, Appl. Opt., 56(15), doi:10.1364/AO.56.004297, 2017.

18 Langille, J., Letros, D., Bourassa, A., Solheim, B., Degenstein, D., Dupont, F., Zawada, D. and Lloyd, N. D.: Spatial heterodyne observations of water (SHOW) from a high-altitude airplane: characterization, performance, and first results, Atmos. Meas. Tech., 12(1), 431–455, doi:10.5194/amt-12-431-2019, 2019.

19 Livesey, N. J., Read, W. G., Wagner, P. A., Froidevaux, L., Lambert, A., Manney, G. L., Valle, L. F. M., Pumphrey, H. C., Santee, M. L., Schwartz, M. J., Wang, S., Fuller, R. A., Jarnot, R. F., Knosp, B. W., Martinez, E. and Lay, R. R.: Earth Observing System (EOS) Aura Microwave Limb Sounder (MLS) version 4.2x level 2 data quality and description document., 2018.

20 Nedoluha, G. E., Kiefer, M., Lossow, S., Michael Gomez, R., Kämpfer, N., Lainer, M., Forkman, P., Martin Christensen, O., Jin Oh, J., Hartogh, P., Anderson, J., Bramstedt, K., Dinelli, B. M., Garcia-Comas, M., Hervig, M., Murtagh, D., Raspollini, P., Read, W. G., Rosenlof, K., Stiller, G. P. and Walker, K. A.: The SPARC water vapour assessment II: Intercomparison of satellite and ground-based microwave measurements, Atmos. Chem. Phys., doi:10.5194/acp-17-14543-2017, 2017.

21 Pan, L., Solomon, S., Randel, W., Lamarque, J. F., Hess, P., Gille, J., Chiou, E. W. and McCormick, M. P.: Hemispheric asymmetries and seasonal variations of the lowermost stratospheric water vapour and ozone derived from SAGE II data, J. Geophys. Res. Atmos., doi:10.1029/97jd02778, 1997.

22 Pan, L. L., Randel, W. J., Gille, J. C., Hall, W. D., Nardi, B., Massie, S., Yudin, V., Khosravi, R., Konopka, P. and Tarasick, D.: Tropospheric intrusions associated with the secondary tropopause, J. Geophys. Res., 114(D10), D10302, doi:10.1029/2008JD011374, 2009.

23 Randel, W. J., Seidel, D. J. and Pan, L. L.: Observational characteristics of double tropopauses, J. Geophys. Res. Atmos., doi:10.1029/2006JD007904, 2007.

24 Ray, E. A., Moore, F. L., Elkins, J. W., Dutton, G. S., Fahey, D. W., Vömel, H., Oltmans, S. J. and Rosenlof, K. H.: Transport into the Northern Hemisphere lowermost stratosphere revealed by in situ tracer measurements, J. Geophys. Res. Atmos., doi:10.1029/1999JD900323, 1999.

25 Riese, M., Ploeger, F., Rap, A., Vogel, B., Konopka, P., Dameris, M. and Forster, P.: Impact of uncertainties in atmospheric mixing on simulated UTLS composition and related radiative effects, J. Geophys. Res. Atmos., 117(D16), n/a-n/a, doi:10.1029/2012JD017751, 2012.

26 Scott, R. K. and Cammas, J. P.: Wave breaking and mixing at the subtropical tropopause, J. Atmos. Sci., doi:10.1175/1520-0469(2002)059<2347:WBAMAT>2.0.CO;2, 2002.

27 Solomon, S., Rosenlof, K. H., Portmann, R. W., Daniel, J. S., Davis, S. M., Sanford, T. J. and Plattner, G. K.: Contributions of stratospheric water vapour to decadal changes in the rate of global warming, Science (80-.)., doi:10.1126/science.1182488, 2010.

28 Ungermann, J., Pan, L. L., Kalicinsky, C., Olschewski, F., Knieling, P., Blank, J., Weigel, K., Guggenmoser, T., Stroh, F., Hoffmann, L. and Riese, M.: Filamentary structure in chemical tracer distributions near the subtropical jet following a wave breaking event, Atmos. Chem. Phys., 13(20), 10517–10534, doi:10.5194/acp-13-10517-2013, 2013.

29 WMO, (1992). International Meteorological Vocabulary. WMO Technical Publication No. 182.

~~29~~30 World Meteorological Organization (1957), Meteorology: A three dimensional science, WMO Bull., 6, 134–138.